Rational Defect Passivation of Cu₂ZnSn(S,Se)₄ Photovoltaics with Solution-Processed Cu₂ZnSnS₄:Na Nanocrystals

Huanping Zhou,[†,‡,§] Tze-Bin Song,[†,‡,§] Wan-Ching Hsu,[†,‡] Song Luo,[†,‡] Shenglin Ye,[†,‡] Hsin-Sheng Duan,[†,‡] Chia-Jung Hsu,[†,‡] Wenbing Yang,[†,‡] and Yang Yang*[,†,‡]

[†]Department of Materials Science and Engineering and [‡]California NanoSystems Institute, University of California, Los Angeles, California 90095, United States

ⓢ *Supporting Information*

ABSTRACT: An effective defect passivation route has been demonstrated in the rapidly growing Cu₂ZnSn(S,Se)₄ (CZTSSe) solar cell device system by using Cu₂ZnSnS₄:Na (CZTS:Na) nanocrystals precursors. CZTS:Na nanocrystals are obtained by sequentially preparing CZTS nanocrystals and surface decorating of Na species, while retaining the kesterite CZTS phase. The exclusive surface presence of amorphous Na species is proved by X-ray photoluminescence spectrum and transmission electron microscopy. With Na-free glasses as the substrate, CZTS:Na nanocrystal-based solar cell device shows 50% enhancement of device performance (∼6%) than that of unpassivated CZTS nanocrystal-based device (∼4%). The enhanced electrical performance is closely related to the increased carrier concentration and elongated minority carrier lifetime, induced by defect passivation. Solution incorporation of extrinsic additives into the nanocrystals and the corresponding film enables a facile, quantitative, and versatile approach to tune the defect property of materials for future optoelectronic applications.

Defects passivation that inhibits detrimental surface charge recombination is one of the key issues for high-performance inorganic optoelectronics, in particular for solution-processed ones.[1] Despite its generality for full-spectrum controllable properties in optics and electronics, solution processing is often associated with the massive presence of defects at the low-crystallinity interfaces, arising from surface dangling bonds and distorted ion arrangements.[2] Although defects passivation for solution-processed optoelectronics might be achieved through thermal annealing or post-doping, high-energy consumption, complex procedures, and heterogeneous ion diffusion are often required to cover the bare interface that traps charge carriers.[3−10] Meanwhile, it remains less explored for a facile homogeneous defects passivation in solution processing, by taking advantage of its increased controllability over surface charge balance,[11,12] to produce uniform passivation both at nanoparticle surface in solution state and within inorganic films in solid state.

Recently, solution processing has been highlighted in the fabrication of earth abundant semiconducting Cu₂ZnSn(S,Se)₄ (CZTSSe) with characteristic decent band gap and large absorption coefficient for next generation photovoltaics.[13−18]

However, the myriad of defect properties, arising from the complex cation ordering arrangement, currently limit the device performance with large deficit in open circuit voltage and short minority carrier lifetime.[15−17] To overcome these challenges, current defects passivation protocols still thoroughly rely on physical deposition of extrinsic doping with alkali metals, which have been proven effective in both CZTS and its analogous Cu(In,Ga)S₂ (CIGS).[19−23]

We report, for the first time, homogeneous solution incorporation of beneficial Na onto the CZTS nanocrystals surface (Scheme 1). In this approach, amorphous sodium

Scheme 1. Schematic Illustration of the Synthesis of CZTS:Na Nanocrystals and the Corresponding Solar Cell Devices

species are directly introduced at CZTS surface to form homogeneous uniform CZTS:Na nanocrystals. This method-ology is conceptually different from previous reports by avoiding the use of rigid substrates of soda-lime glass or high-vacuum evaporation of NaF layer. To synthesize CZTS:Na nanocrystals, we adopt thermolysis method through sequen-tially preparing CZTS nanocrystals and introducing Na species on the surface of CZTS nanocrystals. The exclusive surface presence of Na species is confirmed by X-ray photo-luminescence spectrum (XPS), transmission electron micros-copy (TEM), while CZTS nanocrystals remain in their kesterite phase after Na incorporation. The solar cell device based on CZTS:Na nanocrystals shows the power conversion efficiency (PCE) of 6.1% on borosilicate glass with 350 nm Mo back-contact, which is 50% higher than that of CZTS nanocrystals device. Solution-processed defects passivation with sodium ions increases carrier concentration and elongates minority carrier lifetime, which in turn enhances device performance. The homogeneous solution incorporation strategy may be further

expanded into other photovoltaics with doping species ranging from alkali metals to alkaline metals and even complex salts.

Experimental details are provided in the Supporting Information (SI). In brief, CZTS nanocrystals were synthesized via a modified colloidal synthesis procedure,[24] and the CZTS:Na nanocrystals were sequentially synthesized by the introduction of Na source on the CZTS surface under same batch. In detail, CZTS nanocrystals were prepared by injecting 2 mL 2 M sulfur oleylamine solution into the 10 mL oleylamine solution containing 1.33 mmol $Cu(acac)_2$, 1.22 mmol $Zn(acac)_2$, and 0.75 mmol $Sn(acac)_2Cl_2$ at 225 °C for 30 min. Then an appropriate amount of CF_3COONa in oleic acid solution was injected into CZTS solution and reacted for another 30 min. The reactant molar stoichiometry of Na/(Cu+Zn+Sn) in CZTS:Na nanocrystals was adjusted from 0.5% to 10%, for corresponding composition and structure characterization (10%) and device optimization (0.5% to 2%). Figure 1a,b shows the typical TEM and high-resolution TEM
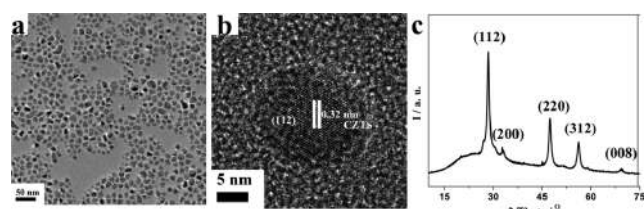

Figure 1. (a) TEM and (b) HRTEM image of the as-prepared CZTS:Na nanocrystals. (c) XRD pattern of the as-prepared CZTS:Na nanocrystals.

(HRTEM) images of the as-prepared CZTS:Na nanocrystals with 10% Na/(Cu+Zn+Sn). The nanocrystals, well dispersed in nonpolar solvent, were highly crystallized with the particle size ranging from 15 to 20 nm. Compared with the CZTS nanocrystals shown in Figure S1a, the slightly smaller size of CZTS:Na particles might be ascribed to both sodium interference to CZTS growth and partially dissolving of the as-formed CZTS nanocrystals. In the HRTEM image of a single CZTS:Na particle (Figure 1b), the center of the particle was highly crystallized with characteristic interplanar distance of 0.32 nm from a (112) plane of kesterite CZTS phase. In contrast, the surface of the nanoparticle was amorphous. Figure 1c shows the X-ray diffraction (XRD) patterns for both CZTS:Na nanocrystals. It is clearly that CZTS:Na nanocrystals exhibited kesterite phase, with the peaks centered at 28.48°, 32.98°, 47.43°, 56.22°, and 69.49° corresponding to the (112), (200), (220), (312), and (008) planes of kesterite (26-0575), respectively. The absence of visible peaks originating from sodium species in the XRD for CZTS:Na nanocrystals suggests that the introduction of amorphous Na on the surface does not change the kesterite phase of CZTS (Figure S1b).

Successful incorporation of Na in the CZTS:Na nanocrystals was further proved by the XPS characterization. The sample for XPS measurement was prepared by spin coating of the as-prepared CZTS:Na into a continuous film with fixed 10% Na/(Cu+Zn+Sn) stoichiometry. As shown in Figure 2a, one strong peak located at 1071 eV, indicative of Na 1s, suggested the existence of Na species in CZTS:Na nanocrystals. Other labeled peaks included Cu (2p 3/2), Zn (2p 3/2), Sn (3d 5/2) and S (2p 3/2) in CZTS. The remaining unlabeled peaks associated with surfactant residues, such as C, O, and N, coming from oleic acid and oleylamine. High-resolution XPS
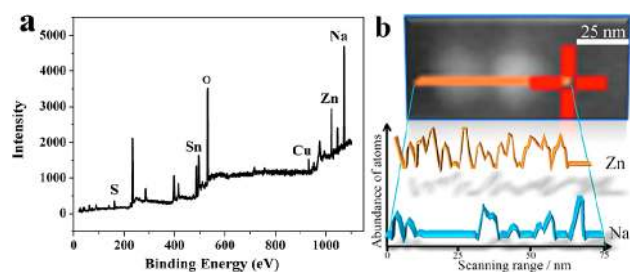

Figure 2. (a) XPS analysis on solution deposited films from the as-prepared CZTS:Na nanocrystals; (b) STEM image (top) of two typical CZTS: Na nanocrystals, scale bar stands for 25 nm and line scan EDS result for Zn and Na in the CZTS: Na nanocrystals (bottom).

scan measurement (Figure S2) further revealed the stoichiometry of each metal element in the CZTS:Na nanocrysals. Much higher ratio of Na/(Cu+Zn+Sn) was determined by XPS measurement, suggesting surface exclusive distribution, rather than homogeneous distribution over the entire nanocrystals, for sodium species. This evidence is also in agreement with the rational design synthesis of CZTS:Na, with stepwisely injection of CF_3COONa.

Scanning transmission electron microscopy (STEM)-energy dispersive spectrum (EDS) measurement was employed for further confirming Na distribution. Figure 2b showed a representative STEM image and line scan EDS result for two typical discrete CZTS:Na nanocrystals. The line scan measurement was carried out in the range of 75 nm, which covered two discrete nanocrystals. The plot of metal composition varied at scanning position was drawn for both Zn and Na atoms. Notably, Zn has a large proportion in CZTS:Na nanocrystals, and no background signal needs to be taken into account. As shown in EDS results, the Na signal strongly localized on the surface of the nanocrystals, and significantly weakened across the center of nanocrystals; whereas, Zn signal kept almost constant along with the entire scan range. Different atomic distribution between Zn and Na further proved surface-exclusive nature of Na, which coincided with the amorphous surface in HRTEM and the absence of sodium-phase in XRD pattern. The incorporation of Na species on nanocrystals surface through colloidal synthesis process is quite different from previously developed Na incorporation strategies, including pretreatment of Mo substrate through vacuum evaporation of NaF layer with certain thickness[8,9] or post-treatment of nanocrystal films through soaking into NaCl solution for several minutes.[10] The vacuum evaporation of NaF layer requires relatively complex procedures, while both reported Na incorporation strategies suffer a longer diffusion length for Na species within the film. It is expected that Na on the nanocrystal surface, with short diffusion length and evenly distribution, can be more favorably to passivate the defects, and against undesired residues in the CZTS film as well.

To study the Na effect on device performance, both CZTS:Na and CZTS nanocrystals were used in the absorber layer of solar cells. The adopted device structure was Mo/CZTS/CdS/Ag-nanowires-ITO, through full solution processing.[25] Detailed device fabrication process is described in the experimental section in SI. The same metal stoichiometry, Cu/Sn = 1.75 and Zn/(Cu+Sn) = 0.6, was used for both CZTS and CZTS:Na nanocrystals. The Na/(Cu+Zn+Sn) ratio was adjusted to 1% for CZTS:Na nanocrystals (Figure S5).

B

dx.doi.org/10.1021/ja407202u | J. Am. Chem. Soc. XXXX, XXX, XXX–XXX

Borosilicate glass was adopted as the substrate to exclude the interference from Na in the substrate. Both CZTS:Na and CZTS nanocrystals were spin-coated to form a continuous film followed by a high-temperature annealing in the presence of selenium.[26,27] Figures 3a and S4 showed the SEM images of the
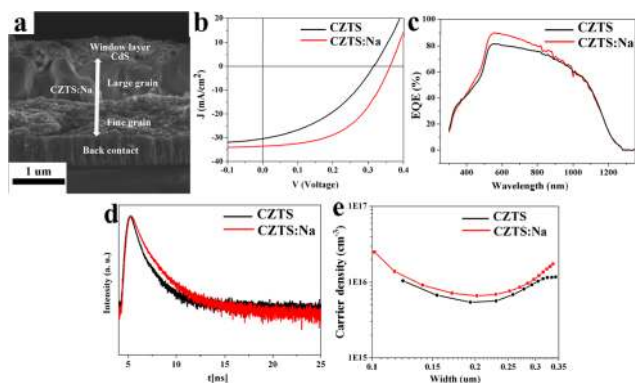

Figure 3. (a) SEM image of typical solar cell based on CZTS:Na nanocrystals. Electrical characterization of the CZTS:Na- and CZTS-based devices: (b) Current−voltage ($J–V$) characteristics under air mass 1.5 illumination, 100 mW/cm^2. (c) EQE spectrum of the device without any applied bias; (d) TRPL of the device under low injection. (e) Capacitance−voltage measurement, with the measurement frequency of 11 kHz, the DC bias ranging from 0 to −0.5 V, and the temperature at 300 K.

two devices. Both devices exhibited identical absorber layer structure with similar thickness of larger grain layer of CZTS, together with certain thickness of fine grain layer. This suggested that Na on the CZTS:Na nanocrystals did not significantly affect the grain growth in the absorber layer. CZTS:Na- and CZTS-based devices exhibited power conversion efficiency values in the range of 5−6% and 3−4%, respectively, as shown in Figure S6. Two typical cell performance data are shown in Figure 3b and Table S1. CZTS:Na-based device showed enhanced open circuit voltage (V_{OC}), short circuit current (J_{SC}) and fill factor (FF) with a much higher PCE (6.14%) than those in CZTS device with 3.89% PCE. Particularly, V_{OC} and FF, which closely related to the carrier recombination, differed significantly within both devices. When the absorber layer changed from CZTS to CZTS:Na, V_{OC} increased 14% from 0.316 to 0.361 V, and FF increased 28% from 39.75% to 50.95%. External quantum efficiencies (EQE) of the two devices are shown in Figure 3c. The superior performance in the CZTS:Na-based device indicates the Na spices have positive effect in CZTSSe photovoltaic devices. This enhancement of device performance, such as V_{OC} and FF, was consistent with the phenomena in previous vacuum-based evaporated NaF method, demonstrating the effectiveness of current solution incorporation of sodium.[8] In addition, with Na inherently existing on the surface of nanocrystals, adhesion problem, coming from the evaporation of NaF film into absorber layer,[28] could be completely avoided. Furthermore, the enhanced device performances clearly demonstrated that the defect passivation in solution could benefit defect passivation in solid state.

The effects from synthetic protocol and Na amount are further investigated, accordingly. First, we explored the effects of reaction time and the reaction temperature during the introduction of Na source. Because the decomposition temperature of Na precursor, CF$_3$COONa, is in the range of

220−270 °C, (Figure S7), we selected the reaction conditions at 225 °C for 15 min or 250 °C for 20 min for the second step reaction, while keeping the synthesis condition for CZTS nanocrystals unchanged. Device performances for CZTS:Na nanocrystals prepared at different conditions are shown in Figure S8. All the electrical parameters for the devices are similar, with the V_{OC} ranging from 0.32 to 0.35 V and FF from 54% to 58%. This suggested the effectiveness of sodium incorporation on both nanoparticle and film states based on thermolysis synthesis. Different Na amounts affected the CZTS:Na-based devices performance significantly. Figure S9 showed the device performance at Na/(Cu+Zn+Sn) reactant stoichiometry of 0.5%, 1%, 1.5%, and 2%, respectively. The performance, V_{OC} and FF, reached its maximum at 1% Na/(Cu+Zn+Sn) and dropped 30% when Na content kept further rising to 2%. At 2% stoichiometry, the formation of sodium-containing impurities in the annealed CZTS film may act as charge trap centers, rather than the effective passivation layer at defects.

To get into the insight of the Na effect on CZTS devices, we used time-resolved photoluminescence (TRPL) and capacitance−voltage (CV) measurement to characterize the minority carrier lifetime and carrier concentration, respectively.[29,30] In the present work, the minority carrier lifetime was obtained from TRPL profiles at low-injection levels (Figure 3d), and 3.6 and 1.5 ns minority carrier lifetime were recorded for the CZTS:Na and CZTS-based devices, respectively. CV measurements for spatial carrier density were also performed with DC bias from 0 V to −0.5 at room temperature, ac level of 5 mV, and measurement frequency of 11 kHZ. The carrier densities for the CZTS:Na- and CZTS-based devices were fitted to be 9−10 and 8−9 × 10^{15} cm$^{−3}$, respectively, as shown in Figure 3e. Higher carrier concentration and longer minority carrier lifetime were both observed in current solution-passivated CZTSSe device. In contrast, evaporation incorporation of Na before the domain growth only raises the carrier concentration on the cost of decreased the minority carrier lifetime.[20] This difference may originate from distinct diffusion length of sodium in the devices. To achieve uniform defect passivation, evaporation passivation requires longer global ion diffusion from interface through the absorber film; whereas solution passivation only requires local diffusion to cover all interfaces within the film. It is possible that the homogeneous Na incorporation adopted in this work initiates a distinguishable mechanism to change the defect chemistry, probably extended from grain boundary to bulk. Further understanding for Na effect on devices based on current solution incorporation is underway.

In conclusion, we report the rational solution passivation of CZTSSe absorber film by the use of solution-processed CZTS:Na nanoparticle precursors. Structure and composition characterizations, including HRTEM, EDS, and XPS, confirm the exclusive presence of sodium species around a kesterite-phase core of CZTS. Specific to solution passivation, both charge carrier concentration and minority lifetime are increased, contributing 50% increment of PCE than that of unpassivated CZTS. Current solution passivation, demonstrated by the simultaneous surface passivation during precursor fabrication, presents a simple, quantitative, and versatile approach toward the pursuit for high-performance photovoltaics. Quantitative introduction of sodium specifies within the absorber layer can be preciously controlled by the reactant stoichiometry; whereas for evaporation, sodium ions are

difficult to diffuse into small cavities that are surrounded by grains. Besides current sodium, other metal ions that can be nucleated onto the core semiconductor materials, including Li, K, and even nonalkali metal or the combinations, may also be explored by simply switching the reactants. Additionally, other photovoltaics, such as CIGS and CdTe thin-film technique, may also be benefit from the solution passivation. Future progress will be focused on the mechanism investigation on the transient charge-transfer behavior within the sodium-passivated absorber film. More importantly, the continuous advance on the extrinsic element doping engineering will enable high-efficiency inorganic photovoltaics and flexible photovoltaics.

■ ASSOCIATED CONTENT

Ⓢ Supporting Information

Detailed experimental procedures and figures. This material is available free of charge via the Internet at http://pubs.acs.org.

■ AUTHOR INFORMATION

Corresponding Author
yangy@ucla.edu
Author Contributions
§These authors contributed equally.
Notes
The authors declare no competing financial interest.

■ ACKNOWLEDGMENTS

■ REFERENCES

(1) Gur, I.; Fromer, N. A.; Geier, M. L.; Alivisatos, A. P. *Science* **2005**, *310*, 462.

(2) Graetzel, M.; Janssen, R. A. J.; Mitzi, D. B.; Sargent, E. H. *Nature* **2012**, *488*, 304.

(3) Luther, J. M.; Law, M.; Song, Q.; Perkins, C. L.; Beard, M. C.; Nozik, A. J. *ACS Nano* **2008**, *2*, 271.

(4) Law, M.; Luther, J. M.; Song, Q.; Hughes, B. K.; Perkins, C. L.; Nozik, A. J. *J. Am. Chem. Soc.* **2008**, *130*, 5974.

(5) Koleilat, G. I.; Levina, L.; Shukla, H.; Myrskog, S. H.; Hinds, S.; Pattantyus-Abraham, A. G.; Sargent, E. H. *ACS Nano* **2008**, *2*, 833.

(6) Beard, M. C.; Midgett, A. G.; Law, M.; Semonin, O. E.; Ellingson, R. J.; Nozik, A. J. *Nano Lett.* **2009**, *9*, 836.

(7) Tang, J.; Kemp, K. W.; Hoogland, S.; Jeong, K. S.; Liu, H.; Levina, L.; Furukawa, M.; Wang, X.; Debnath, R.; Cha, D.; Chou, K. W.; Fischer, A.; Amassian, A.; Asbury, J. B.; Sargent, E. H. *Nat. Mater.* **2011**, *10*, 765.

(8) Li, J. V.; Kuciauskas, D.; Young, M. R.; Repins, I. L. *Appl. Phys. Lett.* **2013**, *102*, 163905.

(9) Prabhakar, T.; Jampana, N. *Sol. Energy Mater. Sol. Cells* **2011**, *95*, 1001.

(10) Guo, Q.; Ford, G. M.; Agrawal, R.; Hillhouse, H. W. *Prog. Photovoltaics* **2013**, *21*, 64.

(11) Yu, M.; Fernando, G. W.; Li, R.; Papadimitrakopoulos, F.; Shi, N.; Ramprasad, R. *Appl. Phys. Lett.* **2006**, *88*, 231910.

(12) Voznyy, O. *J. Phys. Chem. C* **2011**, *115*, 15927.

(13) Katagiri, H.; Jimbo, K.; Maw, W. S.; Oishi, K.; Yamazaki, M.; Araki, H.; Takeuchi, A. *Thin Solid Films* **2009**, *517*, 2455.

(14) Todorov, T. K.; Reuter, K. B.; Mitzi, D. B. *Adv. Mater.* **2010**, *22*, E156.

(15) Barkhouse, D. A. R.; Gunawan, O.; Gokmen, T.; Todorov, T. K.; Mitzi, D. B. *Prog. Photovoltaics* **2012**, *20*, 6.

(16) Todorov, T. K.; Tang, J.; Bag, S.; Gunawan, O.; Gokmen, T.; Zhu, Y.; Mitzi, D. B. *Adv. Energy Mater.* **2013**, *3*, 34.

(17) Repins, I. L.; Romero, M. J.; Li, J. V.; Su-Huai, W.; Kuciauskas, D.; Chun-Sheng, J.; Beall, C.; DeHart, C.; Mann, J.; Wan-Ching, H.; Teeter, G.; Goodrich, A.; Noufi, R. *IEEE J. Photovoltaics* **2013**, *3*, 439.

(18) Yang, W.; Duan, H.-S.; Bob, B.; Zhou, H.; Lei, B.; Chung, C.-H.; Li, S.-H.; Hou, W. W.; Yang, Y. *Adv. Mater.* **2012**, *24*, 6323.

(19) Ishizuka, S.; Yamada, A.; Islam, M. M.; Shibata, H.; Fons, P.; Sakurai, T.; Akimoto, K.; Niki, S. *J. Appl. Phys.* **2009**, *106*, 034908.

(20) Rockett, A. *Thin Solid Films* **2005**, *480−481*, 2.

(21) Wei, S.-H.; Zhang, S. B.; Zunger, A. *J. Appl. Phys.* **1999**, *85*, 7214.

(22) Kronik, L.; Cahen, D.; Schock, H. W. *Adv. Mater.* **1998**, *10*, 31.

(23) Schroeder, D. J.; Hernandez, J. L.; Berry, G. D.; Rockett, A. A. *J. Appl. Phys.* **1998**, *83*, 1519.

(24) Guo, Q.; Hillhouse, H. W.; Agrawal, R. *J. Am. Chem. Soc.* **2009**, *131*, 11672.

(25) Chung, C.-H.; Song, T.-B.; Bob, B.; Zhu, R.; Duan, H.-S.; Yang, Y. *Adv. Mater.* **2012**, *24*, 5499.

(26) Guo, Q.; Ford, G. M.; Yang, W.-C.; Walker, B. C.; Stach, E. A.; Hillhouse, H. W.; Agrawal, R. *J. Am. Chem. Soc.* **2010**, *132*, 17384.

(27) Cao, Y.; Denny, M. S.; Caspar, J. V.; Farneth, W. E.; Guo, Q.; Ionkin, A. S.; Johnson, L. K.; Lu, M.; Malajovich, I.; Radu, D.; Rosenfeld, H. D.; Choudhury, K. R.; Wu, W. *J. Am. Chem. Soc.* **2012**, *134*, 15644.

(28) Edoff, M.; Salome, P. M. P.; Hultqvist, A.; Fjallstrom, V. *Materials Research Society Proceedings*, **2013**, *1538*, DOI: 10.1557/opl.2013.998.

(29) Gunawan, O.; Todorov, T. K.; Mitzi, D. B. *Appl. Phys. Lett.* **2010**, *97*, 233506.

(30) Duan, H.-S.; Yang, W.; Bob, B.; Hsu, C.-J.; Lei, B.; Yang, Y. *Adv. Funct. Mater.* **2013**, *23*, 1466.